Science & Technology Development Journal 2022, 25(2):2432-2438

Open Access Full Text Article

Research Article

Impacts of Ga doping on the structural and thermoelectric properties of ZnO bulks sintered by solid-state reaction

Oanh Kieu Truong Le[1,2,3], Anh Tuan Thanh Pham[1,2,*], Truong Huu Nguyen[1,2], Dung Van Hoang[1,2], Thang Bach Phan[1,2,4], Vinh Cao Tran[1,2]

Use your smartphone to scan this QR code and download this article

ABSTRACT

Introduction: ZnO-based bulk materials are known as high-temperature thermoelectric materials due to their high thermal stability and large Seebeck coefficient. The biggest handicaps of pure ZnO are normally its low electrical conductivity and weak thermoelectric power factor. This work aims to improve the electrical and thermoelectric properties of pure ZnO bulks by Ga doping. **Methods:** Pure ZnO and $Zn_{0.98}Ga_{0.02}O$ bulks were fabricated by a solid-state reaction in air at high temperature. The crystalline and microstructural properties of the samples were analyzed by using X-ray diffraction and field-emission scanning electron microscopy, respectively. The dependence of the electrical conductivity, Seebeck coefficient, and power factor on temperature were recorded by using a commercial LSR-3 system. **Results:** Ga doping increases the carrier concentration and density-of-state effective mass, leading to simultaneous improvements in the electrical conductivity and Seebeck coefficient of ZnO. At 500°C, the thermoelectric power factor of the $Zn_{0.98}Ga_{0.02}O$ bulk is remarkably enhanced by 36% to 169.8 μV/mK^2 compared to ZnO. **Conclusion:** Ga doping shows not only a significant improvement in the power factor but also the potential for reducing the thermal conductivity due to spinel phase segregation. Thus, this work provides a promising solution for controlling the thermoelectric performance of ZnO by doping Ga.

Key words: Thermoelectric properties, Ga-doped ZnO, power factor, crystalline structure, ceramics

[1]*Laboratory of Advanced Materials, University of Science, Ho Chi Minh City, Vietnam*

[2]*Vietnam National University, Ho Chi Minh City, Vietnam*

[3]*Faculty of Physics and Engineering Physics, University of Science, Ho Chi Minh City, Vietnam*

[4]*Center for Innovative Materials and Architecture (INOMAR), Ho Chi Minh City, Vietnam*

Correspondence

Anh Tuan Thanh Pham, Laboratory of Advanced Materials, University of Science, Ho Chi Minh City, Vietnam

Vietnam National University, Ho Chi Minh City, Vietnam

Email: pttanh@hcmus.edu.vn

History

- Received: 2022-04-21
- Accepted: 2022-06-06
- Published: 2022-06-30

DOI : 10.32508/stdj.v25i2.3928

Check for updates

INTRODUCTION

Renewable energy harvesting has been well-known as an essential solution in the current imperative situation of fossil resource depletion and climate change. One of them is thermoelectric (TE) technology, which scavenges electricity from unlimited waste heat sources. The extension ability of TE technology mainly depends on the development of TE semiconductors, including inorganic[1], organic[2], and hybrid materials[3]. Large power production from TE materials is one of the prerequisite requirements for high-efficiency TE harvesting devices[4]. It is characterized by a quantity called the power factor, $PF = S^2\sigma$, where S is the Seebeck coefficient and σ is the electrical conductivity. However, the improvement in the PF is hindered by the opposite dependences on the carrier concentrations of S and σ.

Oxide semiconductors such as ZnO, In_2O_3, $SrTiO_3$, etc., are potential TE inorganic materials due to their good thermal stability and high TE performance[5–8]. Among them, ZnO has attracted much attention owing to its nontoxicity, abundance, and low-cost production[5]. However, pure ZnO normally has low electrical conductivity, leading to a weak power factor[9,10]. There have been many reports on doping foreign elements to improve the TE properties of ZnO[11–14]. Specifically, the IIIA-group elements (Al, Ga, In) are often chosen due to their similar ionic radii to Zn^{2+} and n-type dopant behaviors[15–17]. Most of these studies have preferred to employ spark plasma sintering (SPS) for material synthesis with good densification, nanostructure formation, and high TE performance. However, the biggest drawbacks of the SPS method are its expensiveness, complexity, and small sample size. On the other hand, a traditional synthesis technique, i.e., Solid-state reaction sintering has some advantages, such as simplicity, low cost, and mass production ability. Therefore, the aim of this study is to solve two problems: (i) improving the TE properties of pure ZnO material by dopants and (ii) using a simple method for the sintering process. In this work, we synthesize Ga-doped ZnO bulks by using the solid-state reaction sintering technique. Despite causing a small amount of secondary phase segregation, the Ga dopant shows good incorporation in the ZnO lattice, leading to enhancement in the TE properties of ZnO.

Cite this article : Le O K T, Pham A T T, Nguyen T H, Hoang D V, Phan T B, Tran V C. **Impacts of Ga doping on the structural and thermoelectric properties of ZnO bulks sintered by solid-state reaction**. *Sci. Tech. Dev. J. 2022;* 25(2):2432-2438.

MATERIALS – METHODS

Pure ZnO and Ga-doped ZnO bulks were prepared by solid-state reaction sintering at high temperature. Commercial ZnO (99.9% purity, Merck, Germany) and Ga_2O_3 (99.99% purity, Sigma Aldrich, US) powders were used as starting materials. The powder mixture with a Ga ratio of 2 at% was wet ball-milled for 5 hours (Ceramic Instruments Srl., Italy). After that, the mixture was dried for 24 hours to remove water (Shellab, UK). The dried mixture was uniformly screened through a 100-mesh sieve and then slowly pressed at 14 MPa into 30´30´5 mm^3 pellets by a hydraulic compressor. Finally, the green compact body was continuously sintered for 3 hours at 1400°C in air (NaberTherm 1550, Germany).

The samples were cut into 2´2´15 mm^3 bars to measure temperature-dependent TE properties (Seebeck coefficient, electrical conductivity, power factor) from room temperature to 500°C in a helium gas ambiance (Linseis LSR-3, Germany). The carrier concentration and mobility of the samples were obtained from Hall effect-based measurements at room temperature (Ecopia HMS-3000, Korea). A powder X-ray diffraction apparatus (Bruker D8-Advance, Japan) with the θ-2θ configuration and a CuKa source (0.0154 nm) was employed to analyze the crystalline structure of the samples. The microstructural morphology of the samples was observed by using field-emission scanning electron microscopy (Hitachi SU8010, Japan). Based on the Archimedean method, a density determination kit (Sartorius YDK03, Germany) attached to an electronic precision balance (Sartorius BSA 224S-CW, Germany) was used to investigate the bulk density of the samples. In addition, the mechanical hardness of the samples was determined by using a diamond Vickers indentation probe (Nanovea, US).

RESULTS

Structural characteristics

Figure 1**a** shows that all the bulk samples crystallized with the characteristic orientations of the wurtzite ZnO structure (JCPDS 36-1451). This indicates that the sufficient incorporation of Ga dopant does not destroy the host ZnO lattice. However, some small peaks belonging to the spinel $Ga_2Zn_9O_{12}$ phase (JCPDS 50-0448) are observed in the $Zn_{0.98}Ga_{0.02}O$ bulk. To evaluate the effects of the Ga dopant on the crystalline structure of the bulks, some crystallographic parameters, such as the mean crystal size, lattice constants, unit-cell volume, and residual stress, are considered.

First, the mean crystal sizes (D) of some preferred orientations, as shown in Figure 1 **b**, are determined from Scherrer's formula [18], $D = 0.9l/\cos\theta$, where l is the CuKa X-ray wavelength (0.154 nm), is the full width at half maximum of peaks, and θ is the Bragg diffraction angle. Ga doping significantly improves the crystal size along the (100) plane. In contrast, the crystal size along the (002) plane of $Zn_{0.98}Ga_{0.02}O$ bulk is strongly reduced. Thus, the spinel phase tends to compete with the (002) plane and refine smaller crystals/grains. This was confirmed later through microstructure observation.

ZnO is known as an anisotropic crystal; thus, its electrical conductivity can be mainly contributed by the preferred (100), (002), and (101) planes. Among these planes, the (100) is the m-plane orientation of the wurtzite structure, which is nonpolarized and has good ordering with fewer defects [19]. Thus, crystal growth along the (100) plane can improve the conductivity of ZnO. Indeed, Ga doping significantly increases the crystal size along the (100) plane, as shown in Figure 1 **b**. This can contribute to the enhancement in electrical conductivity for the $Zn_{0.98}Ga_{0.02}O$ bulk, as discussed later in the thermoelectric results.

Second, the lattice constants c and a are calculated from the 2θ position of the (002) and (100) planes, respectively, by using the relationship [20]:

$$\frac{1}{d^2_{(hkl)}} = \frac{4}{3}\left(\frac{h^2+hk+k^2}{a^2}\right) + \frac{l^2}{c^2} \quad (1)$$

where $d_{(hkl)} = l/2\sin\theta$ is the interplanar spacing according to Bragg's law. From these calculations, the c/a ratio and unit-cell volume as given by $V_{cell} = a^2 c\sqrt{3}/2$ are derived.

Third, the residual stress (ε) depends on the lattice constant c, as given by $\varepsilon = A(c - c_o)/c_o$, where c_o is the standard value of stress-free powder (0.52066 nm), and A is deduced from the elastic constants of ZnO (–232.8 GPa) [21]. All the results of the lattice constants, unit-cell volume, and residual stress of the ZnO and $Zn_{0.98}Ga_{0.02}O$ bulks are listed in Table 1.

Upon Ga doping, the c value decreases, while the a value remains nearly unchanged. This leads to a decrease in the c/a ratio of the $Zn_{0.98}Ga_{0.02}O$ bulk. The difference in the c/a ratio tends to broaden compared to the standard value of ZnO (c/a = 1.6033) [22]. Consequently, Ga doping increases the degree of deformation of the ZnO lattice. To make it clearer, V_{cell} and ε are considered. The ε values are positive, indicating that all the bulks have tensile stress. The shrinkage of the unit-cell volume is in good agreement with the increase in tensile stress. This can be explained in terms

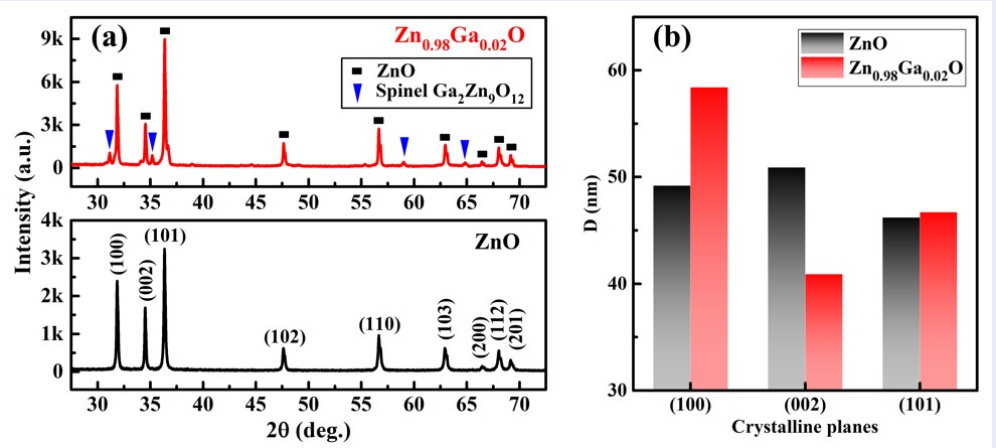

Figure 1: (a) XRD patterns and (b) comparison of the mean crystal size –*D* between the preferred crystalline planes of ZnO and $Zn_{0.98}Ga_{0.02}O$ bulks.

Table 1: Crystallographic information of ZnO and $Zn_{0.98}Ga_{0.02}O$ bulks.

Samples	c (nm)	a (nm)	c/a	Vcell (10-3 nm^3)	ε (GPa)
ZnO	0.5192	0.3241	1.6020	47.2	0.65
$Zn_{0.98}Ga_{0.02}O$	0.5110	0.3240	1.5772	46.5	4.32

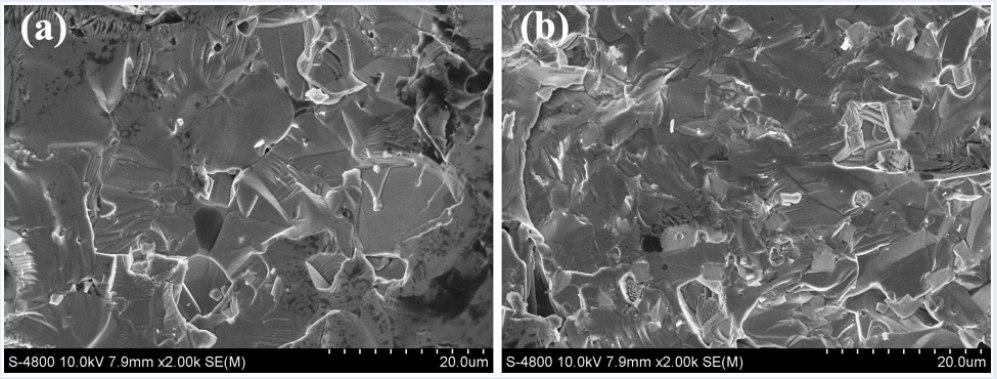

Figure 2: Microstructural morphology of (a) ZnO and (b) $Zn_{0.98}Ga_{0.02}O$ bulks.

of Zn^{2+} substitution by smaller-radius Ga^{3+} (0.074 and 0.068 nm, respectively[23]).

Figure 2 exhibits the microstructural morphology of the bulk samples. The two bulks are well sintered, with high densification. Most of the crystalline grains are large, from several to tens of micrometers in diameter, with long grain boundaries. However, many smaller grains can be observed to be interleaved in the $Zn_{0.98}Ga_{0.02}O$ sample. This can be due to the strong reduction of crystal size along the (002) plane and the spinel phase segregation by Ga doping, which is consistent with the XRD analysis. To support bulk densification, the relative density and hardness of the two samples are investigated.

Figure 3 describes the mechanical properties (density and hardness) of the bulk samples. Based on the Archimedean method, the relative density is determined to be 91.0% TD and 92.3% TD for the ZnO and $Zn_{0.98}Ga_{0.02}O$ bulks, respectively, where TD is the standard density of ZnO material (TD = 5.606 g/cm^3)[24]. The bulk density results indicate that the two samples sintered by the solid-state reaction at high temperature have good densification (>90% TD). Similarly, an increased tendency of hardness is

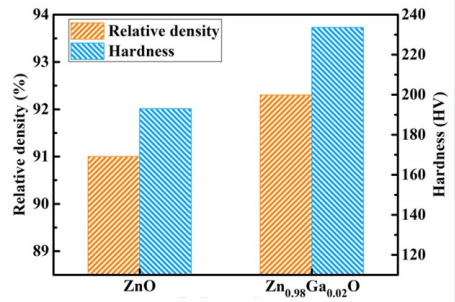

Figure 3: Variation in the relative intensity and hardness of ZnO and $Zn_{0.98}Ga_{0.02}O$ bulks.

observed for the $Zn_{0.98}Ga_{0.02}O$ sample. Combining the XRD, density, and hardness results, it can be suggested that the existence of small grains at interstices and spinel phase segregation in the crystalline microstructure make the $Zn_{0.98}Ga_{0.02}O$ bulk more close-packed, more densified, and harder.

Thermoelectric properties

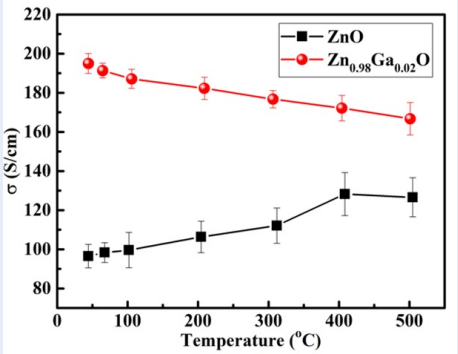

Figure 4: Electrical conductivity –σ of ZnO and $Zn_{0.98}Ga_{0.02}O$ bulks as a function of temperature.

Figure 4 illustrates the dependence of the electrical conductivity of the bulk samples on temperature. The σ of the ZnO bulk increases with temperature, while the value of the $Zn_{0.98}Ga_{0.02}O$ bulk is reversed. This indicates the semiconducting and metallic-like manners of the ZnO and $Zn_{0.98}Ga_{0.02}O$ samples, respectively. When the temperature elevates from room temperature to 500°C, the σ of the $Zn_{0.98}Ga_{0.02}O$ bulk declines by 15% from 195.0 to 166.7 S/cm, which is still greater than that of ZnO. Meanwhile, the σ of the ZnO bulk improves by 31% from 96.5 to 126.6 S/cm. Thus, Ga doping produces donors, resulting in the degeneracy of the semiconducting behavior of the $Zn_{0.98}Ga_{0.02}O$ sample.

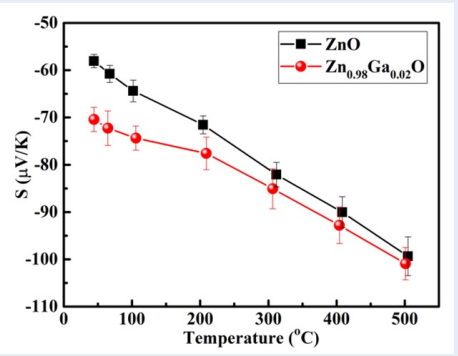

Figure 5: Seebeck coefficient –S of ZnO and $Zn_{0.98}Ga_{0.02}O$ bulks as functions of temperature.

Figure 5 displays the dependence of the Seebeck coefficient of the bulk samples on temperature. All the S values are negative, indicating the n-type majority carriers (electrons) in both samples. The absolute Seebeck coefficient $|S|$ strongly increases with temperature. More concretely, the $|S|$ values of the two bulks have a large difference at low temperature but tend to be asymptotic at high temperature. At 500°C, the $|S|$ values of the $Zn_{0.98}Ga_{0.02}O$ and ZnO bulks are improved to 100.9 and 99.3 μV/K, respectively.

DISCUSSION

In TE materials, the variations in TE parameters (σ, S, …) are not independent but are proportional to each other. Thus, it is necessary to balance these parameters to optimize the TE performance. As shown in Figure 4 and Figure 5, the $Zn_{0.98}Ga_{0.02}O$ bulk has better σ and $|S|$ than the ZnO bulk. Normally, σ is directly proportional to carrier concentration n, while $|S|$ is inversely proportional to n; thus, σ and $|S|$ are opposite to each other. It is expressed by the following relationships:

$$\sigma = n\mu e \tag{2}$$

$$|= \frac{8\pi^2 k_B^2}{3eh^2} m_d^* T \left(\frac{\pi}{3n}\right)^{2/3} \tag{3}$$

where k_B and h are the Boltzmann and Planck constants, respectively; e is the elementary charge; m_d^* is the density-of-state effective mass; and T is the absolute temperature.

From equations (2) and (3), it is difficult to obtain simultaneously high σ and $|S|$ values by increasing n. Thus, the high σ and $|S|$ of the $Zn_{0.98}Ga_{0.02}O$ bulk can be due to the improvement in μ and/or m_d^*. To consider this, the carrier concentration and mobility

Table 2: Comparison of electrical properties obtained from Hall measurement and LSR-3 at room temperature of ZnO and $Zn_{0.98}Ga_{0.02}O$ bulks.

Samples	Hall measurement			LSR-3 measurement	
	n (1019 cm^{-3})	μ (cm^2/Vs)	σ (S/cm)	σ (S/cm)	|S| (μV/K)
ZnO	3.4 ± 0.2	16.7 ± 0.3	90.8 ± 7.1	96.5 ± 6.0	58.1 ± 1.4
$Zn_{0.98}Ga_{0.02}O$	12.1 ± 0.3	11.4 ± 0.5	220.7 ± 15.4	195.0 ± 5.1	70.4 ± 2.6

at room temperature of the two samples are shown in Table 2.

It is seen that the σ obtained from the Hall measurement is consistent with the result from the LSR-3 analysis, with error margins less than 10%. Despite having a high value ($1.2´10^{20}$ cm^{-3}), the | | value of the $Zn_{0.98}Ga_{0.02}O$ bulk is still larger than that of the ZnO bulk. This suggests that the dependence of *S* on the *n* value is minor, and thus, the contribution of m_d^* becomes dominant. This result is compatible with other papers that stated that the incorporation of dopants could increase m_d^* by flattening the conduction or valence band of ZnO[25,26].

In addition, the μ of the $Zn_{0.98}Ga_{0.02}O$ bulk is also reduced compared to that of the ZnO sample. This is explained by the existence of small grains and the spinel phase segregation in the $Zn_{0.98}Ga_{0.02}O$ samples, as demonstrated in the results of the crystalline structure (Figure 1), microstructural morphology (Figure 2), and hardness (Figure 3). Hence, the improvement in σ of the $Zn_{0.98}Ga_{0.02}O$ bulk is attributed to the increase in *n*.

Consequently, Ga doping not only supports free electrons but also increases the density-of-state effective mass, leading to simultaneous improvements in the electrical conductivity and Seebeck coefficient. This facilitates a remarkable enhancement in the TE power factor.

Figure 6 shows the dependence of the power factor of the bulk samples on temperature. The *PF* values of both samples remarkably increase with temperature. Specifically, the *PF* values of the $Zn_{0.98}Ga_{0.02}O$ bulk are maintained to be higher than those of the ZnO bulk over the investigated temperature range. At 500°C, the *PF* values are found to be 169.8 and 124.9 μV/mK^2 for the $Zn_{0.98}Ga_{0.02}O$ and ZnO samples, respectively. This is a result of not only a high electrical conductivity but also a large Seebeck coefficient.

Table 3 lists the TE properties of some previous reports on IIIA-group-doped ZnO bulks. Despite being prepared by a simple solid-state reaction route, the obtained $Zn_{0.98}Ga_{0.02}O$ bulk in this work shows a significantly enhanced power factor. However, this result is still lower than some others, suggesting that the composition and the preparation process have not been optimized.

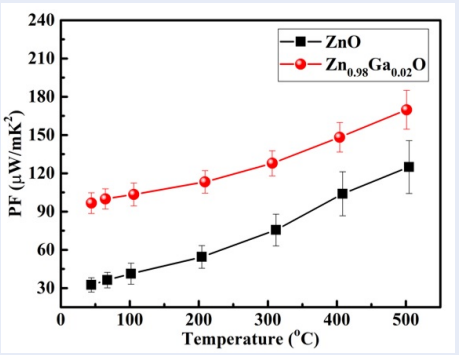

Figure 6: Power factor –PF of ZnO and $Zn_{0.98}Ga_{0.02}O$ bulks as functions of temperature.

CONCLUSION

In this study, the crystalline structure, microstructural morphology, and electrical and thermoelectric properties of pure ZnO and $Zn_{0.98}Ga_{0.02}O$ bulks are investigated. The Ga dopant is not only incorporated into the ZnO lattice but is also segregated in the spinel phase. The incorporation of Ga dopant increases the carrier concentration and density-of-state effective mass, leading to enhanced electrical conductivity and Seebeck coefficient, respectively. As a result, the power factor of the $Zn_{0.98}Ga_{0.02}O$ bulk is improved by 36% to 169.8 μV/mK^2 at 500°C compared to the ZnO bulk. On the other hand, spinel phase segregation tends to refine small crystalline grains, which has the potential for reducing thermal conductivity. The thermal properties of the bulk will be studied in future work.

LIST OF ABBREVIATION

μ: Mobility
σ: Electrical conductivity
n: Carrier concentration
PF: Power factor
: Seebeck coefficient

Table 3: Comparison of the Seebeck coefficient, electrical conductivity, and power factor at 500°C with those of other works.

Materials	Methods	S (μV/K)	σ (S/cm)	PF (μW/mK^2)	Ref.
$Zn_{0.995}Al_{0.005}O$	Solid-state reaction	-310	18	170	[27]
$Zn_{0.99}Al_{0.01}O$		-190	23	83	
$Zn_{0.98}Al_{0.02}O$		-250	100	625	
$Zn_{0.95}Al_{0.05}O$		-175	28	85	
$Zn_{0.9975}Al_{0.0025}O$	Microwaving	-280	25	200	[28]
$Zn_{0.95}Al_{0.05}O$	Coprecipitation	-300	2.2	19.8	[29]
$Zn_{0.995}In_{0.005}O$	Solid-state reaction	-93	430	370	[30]
$Zn_{0.99}In_{0.01}O$		-92	454	380	
$Zn_{0.98}In_{0.02}O$		-90	450	365	
$Zn_{0.95}In_{0.05}O$		-97	256	240	
$Zn_{0.995}In_{0.005}O$	Microwaving	-300	80	720	[31]
$Zn_{0.99}Ga_{0.01}O$	Hydrothermal	-250	33	200	[32]
$Zn_{0.995}Ga_{0.005}O$	Spark plasma sintering	-70	850	420	[33]
ZnO-Ga_2O_3	Solid-state reaction	-95	125	110	[34]
$Zn_{0.98}Ga_{0.02}O$	Solid-state reaction	-100.9	166.7	169.8	This work

TE: Thermoelectric
XRD: X-ray diffraction

COMPETING INTERESTS

The authors declare that they have no competing interests.

AUTHOR CONTRIBUTIONS

Oanh Kieu Truong Le synthesized the samples and wrote the draft. Anh Tuan Thanh Pham performed the measurements and revised the manuscript. Truong Huu Nguyen and Dung Van Hoang took part in the discussion. Thang Bach Phan and Vinh Cao Tran act as scientific supervisors. All the authors have approved the contents of the final version.

ACKNOWLEDGMENTS

This research is funded by University of Science, VNU-HCM under grant number T2021-34.

REFERENCES

1. Hasan MN, Wahid H, Nayan N, Ali MSM. Inorganic thermoelectric materials: A review. Int. J. Energy Res. 2020;44:6170-6222;Available from: https://doi.org/10.1002/er.5313.
2. Wang H, Yu C. Organic thermoelectrics: Materials preparation, performance optimization, and device integration. Joule 2019;3:53-80;Available from: https://doi.org/10.1016/j.joule.2018.10.012.
3. Liang J, Yin S, Wan C. Hybrid Thermoelectrics. Annu. Rev. Mater. Res. 2020;50:319-344;Available from: https://doi.org/10.1146/annurev-matsci-082319-111001.
4. Tanusilp S, Nishide A, Ohishi Y, Muta H, Hayakawa J, Kurosaki K. High thermoelectric power factor of ytterbium silicon-germanium. Appl. Phys. Lett. 2018;113:193901;Available from: https://doi.org/10.1063/1.5047091.
5. Lu N, Zhou C, Wang Y, Elquist AM, Ghods A, Ferguson IT, et al. A review of earth abundant ZnO-based materials for thermoelectric and photovoltaic applications. in Oxide-based Materials and Devices IX (SPIE, 2018);53;Available from: https://doi.org/10.1117/12.2302467.
6. He HF, Zhao B, Qi N, Wang B, Chen ZQ, Su XL, et al. Role of vacancy defects on the lattice thermal conductivity in In2O3 thermoelectric nanocrystals: a positron annihilation study. J. Mater. Sci. 2018;53:12961-12973;Available from: https://doi.org/10.1007/s10853-018-2544-5.
7. Shi X-L, Wu H, Liu Q, Zhou W, Lu S, Shao Z, et al. SrTiO3-based thermoelectrics: Progress and challenges. Nano Energy 2020;78:105195;Available from: https://doi.org/10.1016/j.nanoen.2020.105195.
8. Feng Y, Jiang X, Ghafari E, Kucukgok B, Zhang C, Ferguson I, et al. Metal oxides for thermoelectric power generation and beyond. Adv. Compos. Hybrid Mater. 2018;1:114-126;Available from: https://doi.org/10.1007/s42114-017-0011-4.
9. Duan B, Li Y, Li J, Gao Y, Zhai P, Yang J, et al. Regulation of oxygen vacancy and reduction of lattice thermal conductivity in ZnO ceramic by high temperature and high pressure method. Ceram. Int. 2020;46:26176-26181;Available from: https://doi.org/10.1016/j.ceramint.2020.07.115.
10. Radingoana PM, Guillemet-Fritsch S, Noudem J, Olubambi PA, Chevallier G, Estournès C. Thermoelectric properties of ZnO ceramics densified through spark plasma sintering. Ceram. Int. 2020;46:5229-5238;Available from: https://doi.org/10.1016/j.ceramint.2019.10.271.
11. Sulaiman S, Izman S, Uday MB, Omar MF. Review on grain size effects on thermal conductivity in ZnO thermoelectric materials. RSC Adv. 2022;12:5428-5438;Available from: https://doi.org/10.1039/D1RA06133J.
12. Gayner C, Natanzon Y, Amouyal Y. Effects of codoping and microstructure on charge carrier energy filtering in thermoelectric titanium-doped zinc aluminum oxide. ACS Appl. Mater. Interfaces 2022;14:4035-4050;Available from: https://doi.org/10.1021/acsami.1c20300.
13. Truong DC, Thaowonkaew S, Muthitamongkol P, Horprathum M, Kumar M, Le TBN, et al. Relaxation of residual

stress-controlled thermopower factor in transparent-flexible Ti-doped ZnO thin films. Ceram. Int. 2022;48:2605-2613;Available from: https://doi.org/10.1016/j.ceramint.2021.10.043.
14. Ali HT, Amami M, Rehman U, Mahmood K, Yusuf M, Ikram S, et al. Investigating the thermoelectric power generation performance of ZnCuO: A p-type mixed-metal oxide system. J. Phys. Chem. Solids 2022;163:110535;Available from: https://doi.org/10.1016/j.jpcs.2021.110535.
15. Zhou B, Chen L, Li C, Qi N, Chen Z, Su X, et al. Significant enhancement in the thermoelectric performance of aluminum-doped ZnO tuned by pore structure. ACS Appl. Mater. Interfaces 2020;12:51669-51678;Available from: https://doi.org/10.1021/acsami.0c16506.
16. Jeong A, Ohtaki M, Jang B-K. Thermoelectric performance of In and Ga single/dual-doped ZnO ceramics fabricated by spark plasma sintering. Ceram. Int. 2022;48:14414-14423;Available from: https://doi.org/10.1016/j.ceramint.2022.01.334.
17. Acharya S, Yu B, Hwang J, Kim J, Kim W. High thermoelectric performance of ZnO by coherent phonon scattering and optimized charge transport. Adv. Funct. Mater. 2021;31:2105008;Available from: https://doi.org/10.1016/j.ceramint.2022.01.334.
18. Pham ATT, Nguyen PAT, Phan YKT, Nguyen TH, Hoang DV, Le OKT, et al. Effects of B2O3 doping on the crystalline structure and performance of DC-magnetron-sputtered, transparent ZnO thin films. Appl. Opt. 2020;59:5845;Available from: https://doi.org/10.1364/AO.395051.
19. Doan TLH, Kim J-Y, Lee J-H, Nguyen LHT, Dang YT, Bui K-BT, et al. Preparation of n-ZnO/p-Co3O4 heterojunctions from zeolitic imidazolate frameworks (ZIF-8/ZIF-67) for sensing low ethanol concentrations. Sensors Actuators B Chem. 2021; 348: 130684;Available from: https://doi.org/10.1016/j.snb.2021.130684.
20. Le OKT, Pham ATT, Pham NK, Pham THC, Nguyen TH, Hoang DV, et al. Compensation of Zn substitution and secondary phase controls effective mass and weighted mobility in In and Ga co-doped ZnO material. J. Materiomics 2021;7:742-755;Available from: https://doi.org/10.1016/j.jmat.2020.12.020.
21. Pham ATT, Ngo NM, Le OKT, Hoang DV, Nguyen TH, Phan TB, et al. High-mobility sputtered F-doped ZnO films as good-performance transparent-electrode layers. J. Sci. Adv. Mater. Devices 2021;6:446-452;Available from: https://doi.org/10.1016/j.jsamd.2021.05.004.
22. Özgür Ü, Alivov YI, Liu C, Teke A, Reshchikov MA, Doğan S, et al. A comprehensive review of ZnO materials and devices. J. Appl. Phys. 2005;98:041301;Available from: https://doi.org/10.1063/1.1992666.
23. Nguyen NHT, Nguyen TH, Liu Y-R, Aminzare M, Pham ATT, Cho S, et al. Thermoelectric properties of Indium and Gallium dually-doped ZnO thin films. ACS Appl. Mater. Interfaces 2016;8:33961-33923;Available from: https://doi.org/10.1021/acsami.6b10591.
24. Ewsuk KG, Ellerby DT, Diantonio CB. Analysis of nanocrystalline and microcrystalline ZnO sintering using master sintering curves. J. Am. Ceram. Soc. 2006;89:2003-2009;Available from: https://doi.org/10.1111/j.1551-2916.2006.00990.x.
25. Wu Y, Zhang D-B, Zhao Z, Pei J, Zhang B-P. Enhanced thermoelectric properties of ZnO: C doping and band gap tuning. J. Eur. Ceram. Soc. 2021;41:1324-1331;Available from: https://doi.org/10.1016/j.jeurceramsoc.2020.09.042.
26. Pham ATT, Le OKT, Hoang DV, Nguyen TH, Chen K-H, Park S, et al. Coupling modification of Fermi level, band flattening and lattice defects to approach outstanding thermoelectric performance of ZnO films via tuning In and Ga incorporation. SSRN Electron. J. 2022;Available from: https://doi.org/10.2139/ssrn.4069580.
27. Ullah M, Chunlei W, Su W, Liu D, Zaman A. Thermoelectric properties of Al-doped zinc oxide-based ceramics sintered at high temperature under different atmospheres. J. Mater. Sci. Mater. Electron. 2019; 30: 8611-8618;Available from: https://doi.org/10.1007/s10854-019-01183-6.
28. Jood P, Mehta RJ, Zhang Y, Peleckis G, Wang X, Siegel RW, et al. Al-doped zinc oxide nanocomposites with enhanced thermoelectric properties. Nano Lett. 2011; 11: 4337-4342;Available from: https://doi.org/10.1021/nl202439h.
29. Mayandi J, Madathil RK, Abinaya C, Bethke K, Venkatachalapathy V, Rademann K, et al. Al-doped ZnO prepared by co-precipitation method and its thermoelectric characteristics. Mater. Lett. 2021; 288: 129352;Available from: https://doi.org/10.1016/j.matlet.2021.129352.
30. Ullah M, Chunlei W, Su W-B, Manan A, Ahmad AS, Rehman AU. Thermoelectric properties of indium-doped zinc oxide sintered in an argon atmosphere. J. Mater. Sci. Mater. Electron. 2019; 30: 4813-4818;Available from: https://doi.org/10.1007/s10854-019-00775-6.
31. Jood P, Mehta RJ, Zhang Y, Borca-Tasciuc T, Dou SX, Singh DJ, et al. Heavy element doping for enhancing thermoelectric properties of nanostructured zinc oxide. RSC Adv. 2014; 4: 6363;Available from: https://doi.org/10.1039/C3RA46813E.
32. Jantrasee S, Moontragoon P, Pinitsoontorn S, Ruttanapun C. Enhancing thermoelectric properties of nanostructure Ga-doped ZnO prepared by microwave-hydrothermal synthesizing with comparing to calculation results. Mater. Res. Express 2019; 6: 045047;Available from: https://doi.org/10.1088/2053-1591/aafc39.
33. Jung KH, Hyoung Lee K, Seo WS, Choi SM. An enhancement of a thermoelectric power factor in a Ga-doped ZnO system: A chemical compression by enlarged Ga solubility. Appl. Phys. Lett. 2012; 100: 2010-2014;Available from: https://doi.org/10.1063/1.4729560.
34. Michiue Y, Nishijima H, Suzuki Y, Mori T. Synthesis and thermoelectric properties of composite oxides in the pseudobinary system ZnO-Ga2O3. Solid State Sci. 2017; 65: 29-32;Available from: https://doi.org/10.1016/j.solidstatesciences.2016.12.020.